

Numerical modelling of shielding gas flow and heat transfer in laser welding process

Alireza Javidi Shirvan¹, Isabelle Choquet¹, Håkan Nilsson²

¹University West, Department of Engineering Science, Trollhättan, Sweden

²Chalmers University of Technology, Department of Applied Mechanics, Gothenburg, Sweden
alireza.javidi@hv.se

ABSTRACT

In the present work a three-dimensional model has been developed to study shielding gas flow and heat transfer in a laser welding process using computational fluid dynamics. This investigation was motivated by problems met while using an optical system to track the weld path. The aim of this study was to investigate if the shielding gas flow could disturb the observation area of the optical system. The model combines heat conduction in the solid work piece and thermal flow in the fluid region occupied by the shielding gas. These two regions are coupled through their energy equations so as to allow heat transfer between solid and fluid region. Laser heating was modelled by imposing a volumetric heat source, moving along the welding path. The model was implemented in the open source software OpenFOAM and applied to argon shielding gas and titanium alloy Ti6Al4V base metal. Test cases were done to investigate the shielding gas flow produced by two components: a pipe allowing shielding the melt, and a plate allowing shielding the weld while it cools down. The simulation results confirmed that these two components do provide an efficient shielding. They also showed that a significant amount of shielding gas flows towards the observation area of the optical system intended to track the weld path. This is not desired since it could transport smoke that would disturb the optical signal. The design of the shielding system thus needs to be modified.

Keywords: laser welding, shielding gas, volumetric heat source, coupling boundary

1 Introduction

This study was motivated by problems met in a manufacturing context while welding titanium with a laser welding tool. In this welding process a shielding gas is brought by a pipe above the base metal around the focal point of the laser heat source. The first reason for using a shielding gas is to prevent the molten metal from the harmful effect of the ambient air [1]. The oxygen and nitrogen present in the air can cause slag inclusions and brittleness, respectively. Helium, argon

and carbon dioxide are the most common shielding gases in welding. Argon is an appropriate option for sensible materials such as aluminium, stainless steel, and titanium [1], since it does not react chemically with welded materials. Argon is the shielding gas used in this study.

When welding materials that are highly reactive with oxygen, a shielding gas can also be used to form an additional screen large enough to cover the part of the weld already solidified but not yet cooled. In this study a plate is fixed on the back side of the pipe (see

Fig. 1) to form an argon shielding screen covering the weld and preventing titanium from oxidizing during cooling. The welding apparatus is planned to be equipped with an optical system intended to track the welding path. The optical system must be mounted in front of the welding tool to observe the front area of the weld.

During welding smoke is emitted. This smoke is a mixture of fine particles (fume) and gases produced in the weld. It flows under the combined action of buoyancy force and the surrounding shielding gas flow. The problem motivating this study is that the smoke could flow through the observation area of the optical system used to track the weld path, and thereby affect the accuracy of the path tracking. A better knowledge of the shielding gas flow was thus needed.

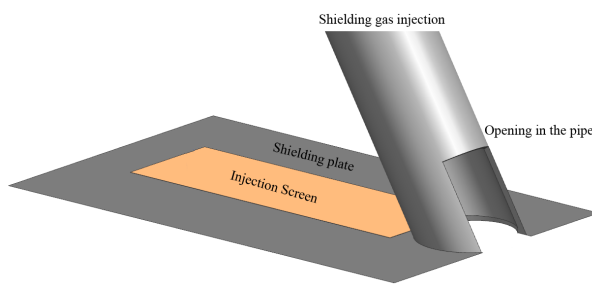


Figure 1: Schematic sketch of the shielding plate for case 4

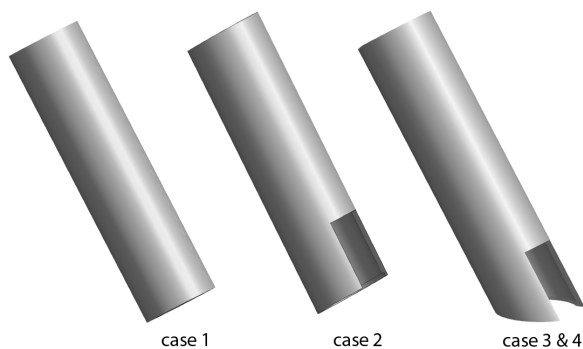


Figure 2: shielding pipe for different cases

The present work was done to study the shielding gas flow investigating both the shielding gas injected by the shielding pipe and the extended shielding screen. As these gas flows are partially hidden by the equipment, a convenient way to study them was to perform simulations using computational fluid dynamics (CFD).

Some studies based on CFD [2, 3] have been done to understand the fluid dynamics of the shielding gas during laser welding process. Hong et al. [2] considered argon and helium as shielding gas with three different ranges of flow rate through a circular pipe with two different angles with the work piece. Tani et al. [3] have tested four different types of gas with three different pipe angles and three different flow rates to study the influence of each parameter on the behaviour of the shielding gas flow. Shuja et al. [4] used air for gas injection rather than a usual shielding gas, and considered different welding speed. However, the influence of the plate used to form an extended shielding screen was not investigated by these authors.

The present work, was done using the OpenFOAM-1.6.x OpenSource CFD tool (www.openfoam.com). OpenFOAM is basically a general library of C++ classes for numerical simulation of continuum mechanic problems, and it is mainly used in CFD. The simulation model implemented in OpenFOAM combines heat conduction in a solid region (the work piece) and thermal flow in a fluid region (occupied by the shielding gas). A thermal energy equation is thus solved in the solid region. In the fluid region a larger set of equations including mass, momentum and energy conservation is solved. These two regions are coupled through their energy equations so as to allow heat transfer between solid and fluid region. This coupling is also called conjugate heat transfer. The laser is modelled as a heat source acting locally on the surface of the work piece.

The model for shielding gas flow and laser heat source is discussed in section 2. In section 3, the test cases and numerical settings are given. The first test cases are done for pipes that are not equipped with a plate. The angle between pipe axis and work piece is 60° . The geometry of the first pipe simulated (see Fig. 2, left) has an end opening normal to the pipe axis but no lateral opening. This configuration cannot be used in practice, as it would not allow the laser beam to reach the work piece. This test case was however studied

since it gives information on the influence of the lateral opening of the pipe on the shielding gas flow. The second and the third pipe configuration tested have, in addition of the end opening, a lateral opening allowing the laser beam to reach the work piece (see Fig. 2, centre and right). Their difference lies in the angle between the pipe end opening and the pipe section: 0° in the second case, and 30° in the third case. In the last test case, the shielding pipe is equipped with a plate for forming an extended shielding screen. The plate includes in its central part an injection screen to inject shielding gas (see Fig. 1). The simulation results are discussed in section 4.

2 Model

The domain plotted in Fig. 3, is divided into two different parts: the solid part, and the fluid part. The solid domain is made of Ti6Al4V alloy and the fluid part contains pure argon gas. The fluid part contains the shielding pipe and in case 4 the shielding plate too. A 3D model was implemented to solve the flow dynamics and heat conduction equations in the fluid and solid parts respectively. The following assumptions have been made:

1. Based on the characteristic velocity and temperature of this study, the maximum Mach number of the fluid flow is $Ma = 0.014$. As the maximum Mach number is less than 0.3, the flow is assumed incompressible.
2. As the fluid is argon, it is assumed to be Newtonian.
3. In the fluid part, the thermodynamic and transport properties of the shielding gas are assumed to be constant, since they vary very little over the temperature range studied.
4. Assuming a smooth pipe wall, the shielding gas flow rate and the pipe diameter lead to a Reynolds number of $Re \simeq 3.5 \times 10^3$. This means a flow in transient regime. For simplicity, a laminar flow is considered in the model.
5. The surface of the work piece is assumed to be flat, melting is not considered, and thermodynamic properties are assumed constant.

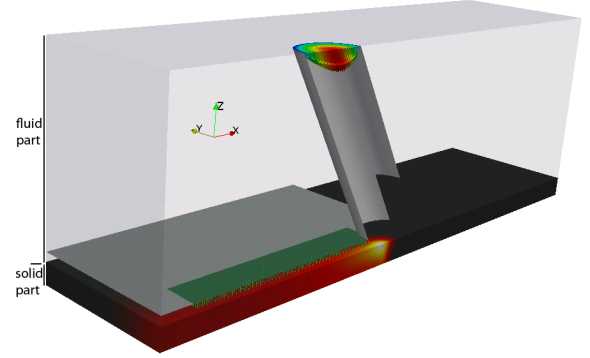


Figure 3: Schematic sketch of a section of the model

2.1 Governing equations in the fluid part

The system of equations governing the flow is the set of steady laminar Navier-Stokes equations for an incompressible and thermal fluid. This set is expressed in cartesian coordinates (x, y, z) . In the sequel, x denotes the location along the welding direction, z along the direction through the solid and y is the location perpendicular to the two former (see Fig. 3). The mass conservation equation is given by

$$\frac{\partial}{\partial x_i}(\rho^f U_i) = 0 \quad (1)$$

where ρ^f is the fluid density and U_i refers to the i^{th} component of the fluid velocity. The conservation of momentum is given by

$$\frac{\partial}{\partial x_j}(\rho^f U_i U_j) - \frac{\partial}{\partial x_j} \left(\mu \frac{\partial U_i}{\partial x_j} \right) = -\frac{\partial p}{\partial x_i} \quad (2)$$

where p is the pressure and μ is the viscosity of the fluid. As argon is light, the gravitational force is negligible. The conservation of enthalpy is given by

$$\frac{\partial}{\partial x_i}(\rho^f U_i h) - \frac{\partial}{\partial x_i} \left(k^f \frac{\partial h}{\partial x_i} \right) = 0 \quad (3)$$

where k^f is the thermal conductivity of the fluid and h is the enthalpy. As can be seen, this equation implies that there is no heat generation in the fluid. It is because the heat is generated in the solid part and transferred to the fluid through diffusion.

2.2 Governing equation in the solid part

The governing heat conduction equation accounting for laser heating can be written as

$$U_i^r \frac{\partial}{\partial x_i} (\rho^s c_p^s T) - \frac{\partial}{\partial x_i} (K^s \frac{\partial T}{\partial x_i}) = Q_{ls} \quad (4)$$

where U_i^r is the i^{th} component of the relative velocity of the work piece with respect to the laser heat source. ρ^s is the solid density, c_p^s the specific heat at constant pressure, K^s the thermal conductivity of the solid material, and Q_{ls} the laser heat source.

The solution for the heat conduction equation for a moving heat source was studied by VanElsen et al. [5].

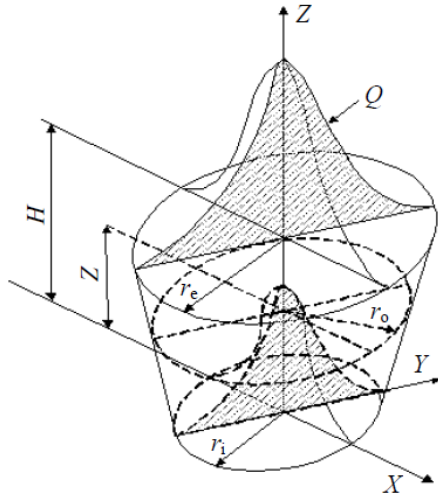


Figure 4: Heat source power density distribution [6]

A gaussian laser energy distribution is commonly used to model the laser heat source [6, 7]. In this study the volumetric laser heat source Q_{ls} is modelled according to Chuan et al. [6], i.e.

$$Q_{ls}(x, y, z) = \frac{2\eta P}{\pi r_e^2 H} \exp\left(\frac{-r^2}{r_0^2}\right) \quad (5)$$

$$r^2 = x^2 + y^2$$

$$r_0 = r_i + \frac{(r_e - r_i)z}{H}$$

where η is the thermal efficiency, P the laser power and r_e and r_i are the half width of the weld at the top

and bottom surface, respectively. In this study, which is concerned with full penetration laser welding, the welding penetration H is the thickness of the work piece, see Fig.4.

3 Cases and numerical settings

The parameters needed to set the test cases were taken from the manufacturing application. The thickness of the work piece is 7 mm , its length is 200 mm and its half-width is 50 mm . A pipe with 20 mm diameter is included in the model to inject argon with the flow rate of 45 l/min . The pipe makes a 60° angle with the horizontal line, see Fig. 5.

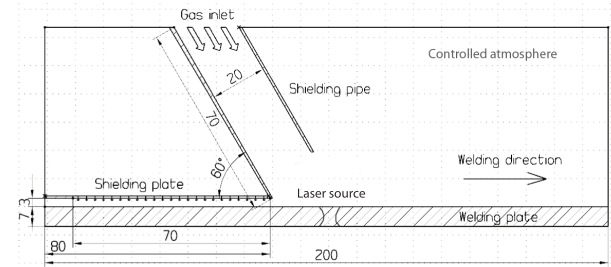


Figure 5: Partial cross section of the model [mm]

The velocity of the moving heat source is 800 mm/min . The heat source models a TEM_{00} laser source with a power of 2500 W . A thermal efficiency of 100% is considered and the width of the weld at top and bottom of the fusion zone are 7 mm and 3 mm respectively.

The density, viscosity and thermal conductivity of the argon shielding gas are

$$\rho^f = 0.686\text{ kg m}^{-3},$$

$$\mu = 0.432 \times 10^{-4}\text{ kg m}^{-1}\text{ s}^{-1},$$

$$k^f = 0.0338\text{ W m}^{-1}\text{ K}^{-1}.$$

The density, specific heat and thermal conductivity of the titanium alloy work piece are

$$\rho^s = 4309\text{ kg m}^{-3}$$

$$C_p^s = 714\text{ J kg}^{-1}\text{ K}^{-1},$$

$$K^s = 17.8\text{ W m}^{-1}\text{ K}^{-1}.$$

To study the shielding gas behaviour over the work piece, four different cases have been tested. Three

cases aim at investigating the effect of the shielding pipe outlet shape on the gas flow without shielding plate, see Fig.2. The fourth case is inspecting the influence of the shielding plate on the gas flow, see Fig.1.

Case 1 includes the left pipe of Fig. 2 and no shielding plate. This first pipe has an end opening normal to the pipe axis but no lateral opening. This configuration cannot be used in practice, as it would not allow the laser beam to reach the work piece. This test case was however studied since it gives information on the influence of the lateral opening of the pipe on the shielding gas flow.

As can be seen in Fig. 2 the shielding pipe of case 2 is based on case 1 but with the presence of an additional opening on the wall of the pipe to let the laser beam reach the base metal (see Fig. 2, centre). The dimension of the opening is $13\text{ mm} \times 20\text{ mm}$.

Case 3 differs from case 2 by the shape of the outlet of the pipe. (see Fig. 2, right). The angle between the pipe end opening and the pipe section is equal to 30° in the third case while it was equal to 0° in the former cases.

The model in case 4 is implemented with the same features as case 3, supplemented with a shielding plate. The shielding plate has an injection screen through which the gas flows at a rate of 45 l/min to cover the welded part, see Fig.1. The injection screen of the shielding plate has a length of 70 mm and an half-width of 20 mm . The geometry of the model is illustrated by the cross-section in Fig. 5.

The meshes of cases 1 to 3 have about 3.3 million cells. Case 4 has only about 1.4 million cells since the region located over the shielding plate and behind the pipe does not need to be included into the computational domain.

3.1 Boundary conditions

Boundary conditions are applied for the fluid part, the solid part, and the interface between them.

3.1.1 Fluid part

A parabolic velocity distribution is specified at the inlet of the shielding pipe. To achieve the flow rate of 45 l/min , a maximum velocity of 4.77 m/s is employed.

In case 4, where the shielding plate is included, an inlet boundary with uniform velocity of 1.9 m/s is also set at the injection screen to form a shielding screen with a flow rate of 45 l/min .

At the surrounding boundaries of the fluid part (on top and sides), a zero gradient condition is used for the velocity and the pressure is set to the atmospheric pressure.

The inlet temperature of the shielding gas is at room condition, that is 300 K . The same temperature condition is applied to the fluid boundaries (on top and sides) of the computational domain.

It was checked (running calculations with a larger computational domain) that the size of the computational domain is large enough to allow using such boundary conditions.

3.1.2 Solid part

In the manufacturing application, cooling water was flowing into a duct mounted under the work piece. The water inlet temperature was 6° C . The details of the cooling system were not included in the simulation model. The cooling effect was accounted for in a simplified way in the simulation test, assuming a fixed temperature condition $T = 300\text{ K}$ at the bottom solid boundary. This value was calculated using standard analytic models for heat transfer in pipe flow. A zero gradient boundary condition is employed for the temperature at the sides of the solid part.

3.1.3 Interface between solid and fluid

At the interface between the solid and fluid regions, a common no-slip boundary condition is set for the fluid velocity.

Solid and fluid are coupled through their energy equations so as to allow heat transfer between solid and fluid region. The energy equation in the solid region governs the solid temperature, while the energy equation in the fluid region governs the fluid enthalpy. So their coupling is not direct: the direction of the heat flux is first determined. Then, the thermal coupling is done setting automatically the fixed value or the fixed gradient depending on the direction of the heat flux. This boundary condition, called a conjugation boundary for heat flux and temperature, is implemented by a solver so called `chtMultiRegionFoam` in `OpenFOAM 1.6x`.

The open source software, OpenFOAM-1.6.x was employed to run the simulations based on above three-dimensional configurations.

4 Results

4.1 Temperature distribution

Fig. 6 represents the temperature distribution over the base metal and through the work piece in case 4. As the model does not yet account for phase change, the maximum temperature raises up to 2100 K which is higher than the melting point of titanium alloy Ti6Al4V which is about 1900 K .

The temperature distribution over the work piece along the x-axis is plotted for case 3 and case 4 in Fig. 7. The x-axis is located at the intersection of the symmetry plane and the top surface of the solid region. It can be observed in Fig. 7 that the weld temperature decreases strongly, by about 1300 K , over a short distance from the laser heat source ($40 < x < 90\text{ mm}$). In this region, the cooling rates of case 3 and 4 are almost the same. The extension of the heat affected zone is less than $1/10^{\text{th}}$ of shielding screen area. So the volume flow rate of argon flowing effectively above the heat affected zone in case 4 is less than 4.5 l/min . A plot of the the velocity field in a cross-section under the shielding plate in $x = 50\text{ mm}$ shows that above the weld (on the left hand side of Fig.8) the velocity of the shielding gas is very small. The shielding gas has thus in this region a poor ability to cool down by convective heat transfer. As a result, the presence of the shielding screen in this area does not improve the cooling.

Further away from the laser heat source (in $0 < x < 40\text{ mm}$) the velocity of the shielding gas above the weld is slightly larger, see Fig. 9 on the left. The cooling by convective heat transfer is thus slightly larger. Accordingly, in this region the solid surface temperature is almost 20 K lower in case 4 than in case 3.

To conclude this part, the shielding plate does not provide any significant additional cooling of the weld. The shielding plate was indeed designed to protect the weld from the surrounding air, and not to further increase the cooling rate.

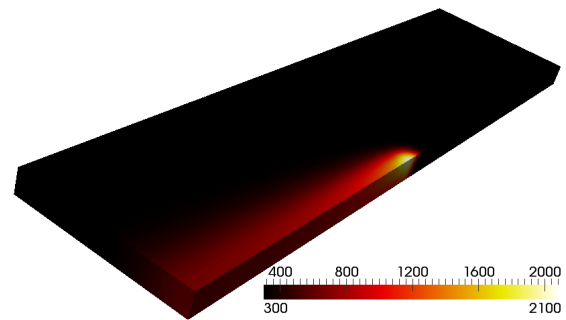


Figure 6: Temperature [K] distribution in the solid plate - case 4

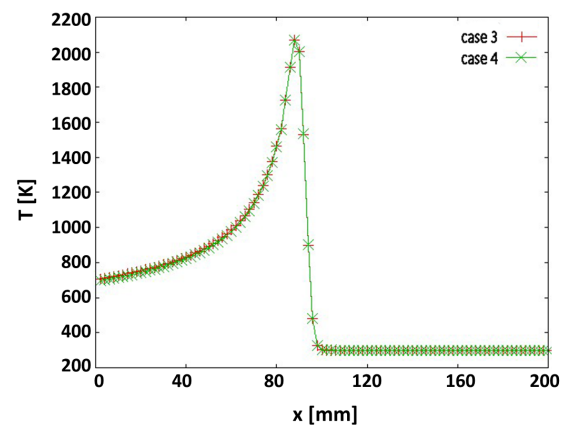


Figure 7: Temperature at the solid surface at the symmetry plane

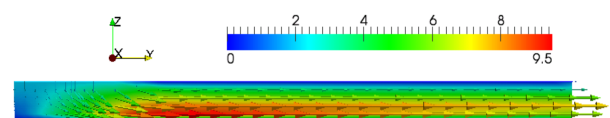


Figure 8: Velocity [m/s] in the cross section $x = 50\text{ mm}$ of the shielding plate, case 4. The left hand side is at the symmetry plane. The right hand side is at the edge of the shielding plate.

4.2 Velocity distribution

To compare the results obtained with the different test cases, the magnitude of the velocity is plotted in the symmetry plane.

Comparing Figs. 10 top and bottom reveals that the velocity profile and magnitude in case 1 and case 2 have almost the same patterns and values. The argon gas injected in the pipe is not pressurized. Pressure gradients along the radial direction from pipe axis to the surroundings are thus negligible at some distance above the work piece. Closer to the work piece the argon pipe jet is deflected because of the presence of the base material surface. As the pipe end opening and the work piece make an angle of 30° , the open space is large enough for the argon jet to be deflected without disturbing significantly the flow inside the pipe and thus in the lateral pipe opening. So, with the configuration of case 2, the opening on the pipe wall does not affect significantly the shielding gas distribution compared to case 1. Increasing enough the volume flow rate of the shielding gas, or reducing enough the angle between the pipe end opening and the work piece, would change this result.

The magnitude of the velocity obtained with the test case 3 is plotted in Fig.11. Fig.11 shows that when reducing the angle between the pipe end opening and the work piece down to 0° , the shielding gas flow behaves differently and a higher velocity is achieved over the base metal. So this pipe configuration is less favourable than the configuration of case 2, since a higher shielding gas velocity towards the front of the weld will most probably entrain more smoke in the observation area of the optical system intended to track the welding path.

The velocity fields of case 4, plotted in Fig. 8 and Fig. 9, confirm that the protection against the oxidizing surrounding atmosphere is achieved by the shielding screen since the shielding gas prevents the atmosphere from flowing towards the weld.

Fig. 12 is a zoom at the junction between pipe and shielding plate, showing the velocity vectors of the shielding gas in the symmetry plane. It indicates that part of the shielding screen (from the plate) flows towards the pipe, joins the pipe flow and thus increases the amount of gas flowing towards the front of the weld. This flow can entrain even more smokes and fumes towards the front of the weld and the observation area of the optical system.

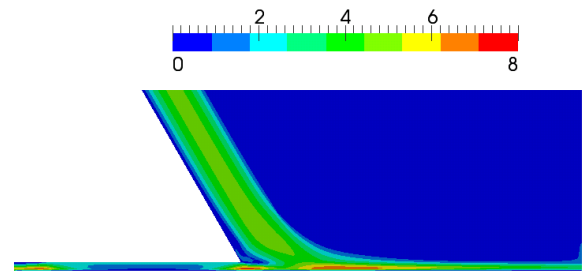


Figure 9: Velocity [m/s] at the symmetry plane case 4.

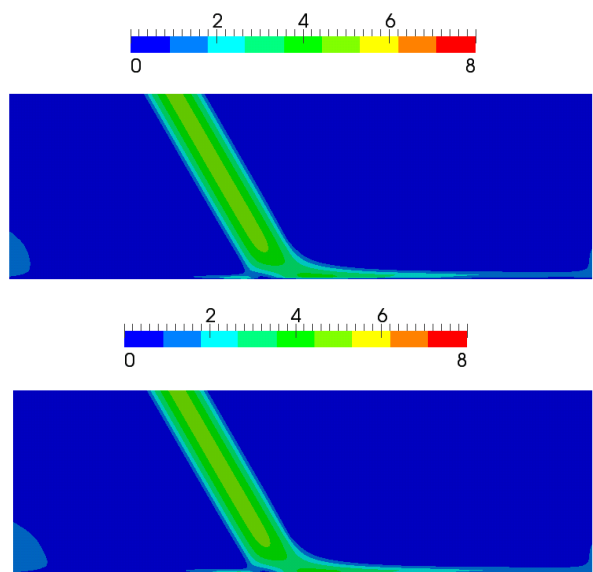


Figure 10: Velocity [m/s] at the symmetry plane.
Top: case 1, bottom: case 2

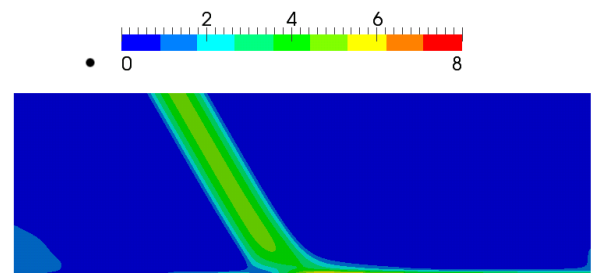


Figure 11: Velocity [m/s] at the symmetry plane case 3

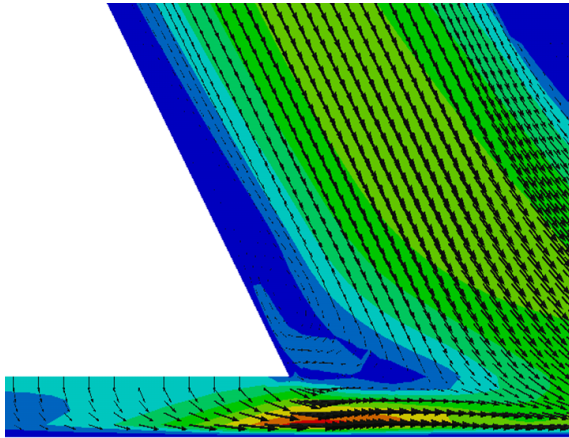


Figure 12: Zoom of case 4 showing the velocity vectors in the symmetry plane, at the junction between pipe and shielding plate.

5 Conclusions

The flow of the laser welding shielding gas over the base metal with both shielding pipe and shielding plate has been studied. The present results confirm that the shielding plate provides a good protection of the cooling weld against the surrounding atmosphere.

The shielding screen produced by the plate has a negligible influence on the cooling rate of the weld.

However, the design of the shielding pipe and plate (case 4, the case used in practice) is in conflict with the requirements of the optical system for tracking the welding path. A larger angle between end pipe opening and work piece, as in case 2, leads to lower shielding gas velocity towards the front of the weld compared to case 3 (and 4), but this is not sufficient to protect the observation area from the possible entrainment of fumes by the shielding gas. Based on case 2, more extended lateral openings on the pipe wall are not expected to provide any significant improvement. The design of the pipe and plate should thus be modified to deflect differently the shielding gas flow, away from the observation area, while maintaining a proper shielding. A solution could be to force a lateral flow of the shielding gas by introducing pressure gradients.

Checking with CFD that a new design is suited will require a more detailed modelling of the flow, accounting for turbulence, as the pipe flow is known to be transient (see section 2), and turbulence may also disturb

the observation area of the optical system for tracking the welding path.

6 References

- [1] K.Weman (2003). *Welding processes handbook*. Woodhead publishing ltd. England.
- [2] H.Wang, Y.Shi, S.Gong, A.Duan (2007). Effect of assist gas flow on the gas shielding during laser deep penetration welding. *Journal of Material processing Technology*. **184**, pp. 379-385.
- [3] G.Tani, A.Ascari, G.Campana, A.Fortunato (2007). A study on shielding gas contamination in laser welding of non-ferrous alloys. *Applied Surface Science*. **254**, pp. 904-907.
- [4] S.Z.Shuja, B.S.Yillbas,(2000). 3-Dimensional conjugate laser heating of a moving slab. *Applied surface science*. **167**, pp. 134-148.
- [5] M.Van Elsen, M.Baelmans, P.Mercelis, J.-p. Kruth (2007). Solution for modelling moving heat source in a semi-infinite medium and applications to laser material processing. *International Journal of heat and mass transfer*. **50**, pp. 4872-4882.
- [6] L.Chuan, Z.Jianxun, N.Jing (2009). Numerical and Experimental Analysis of Residual Stresses in Full-Penetration Laser Beam Welding of Ti6Al4V Alloy. *Rare Metal Materials and Engineering*. **38**, pp. 1317-1320.
- [7] K.Abderrazak, W.Kriaa, W.Ben Salem, H.Mhiri, G.Lepalec, M.Autric (2009). Numerical and Experimental studies of molten pool formation during an interaction of a pulse laser (ND:YAG) with a magnesium alloy. *Optics and Laser technology*. **41**, pp. 470-480.